

New channel to search for dark matter at Belle II

Jinhan Liang,^{a,b,c} Zuwei Liu^{a,d} and Lan Yang^a

^a*Department of Physics, Nanjing University, Nanjing 210093, China*

^b*Guangdong Provincial Key Laboratory of Nuclear Science, Institute of Quantum Matter, South China Normal University, Guangzhou 510006, China*

^c*Guangdong-Hong Kong Joint Laboratory of Quantum Matter, Southern Nuclear Science Computing Center, South China Normal University, Guangzhou 510006, China*

^d*CAS Center for Excellence in Particle Physics, Beijing 100049, China*

E-mail: jinhanliang@smail.nju.edu.cn, zuweiliu@nju.edu.cn,
lanyang@smail.nju.edu.cn

ABSTRACT:

We propose a new “disappearing positron track” channel at Belle II to search for dark matter, in which a positron that is produced at the primary interaction vertex scatters with the electromagnetic calorimeter to produce dark matter particles. Such scatterings can occur via either annihilation with atomic electrons, or the bremsstrahlung process with target nuclei. The main backgrounds are due to photons and neutrons that are produced in the same scatterings and then escape detection. We require a large missing energy and further veto certain activities in the KLM detector to suppress such backgrounds. To illustrate the sensitivity of the new channel, we consider a new physics model where dark matter interacts with the standard model via a dark photon, which decays predominantly to dark matter; we find that our proposed channel can probe some currently unexplored parameter space, surpassing both the mono-photon channel at Belle II and the NA64 constraints.

Contents

1	Introduction	1
2	Disappearing positron track	3
3	Standard Model Backgrounds	4
3.1	Photon-induced backgrounds	5
3.2	Neutron-induced backgrounds	6
4	Sensitivity on dark matter in dark photon models	7
5	Conclusions	10
A	Track-length distribution of positrons and electrons	11
B	Dependence of signal on α_D	12
C	NA64 constraints	13
D	SM backgrounds due to charged particles	13
E	Sensitivity on the scalar mediator model	15
F	Sensitivity of the radiative Bhabha scattering process	16

1 Introduction

Dark matter (DM) is one of the most fundamental and longstanding questions in modern physics [1]. However, the particle property of DM remains elusive, despite the overwhelming evidence of its gravitational effects [1–4]. Particle colliders are one of the most powerful tools to search for DM. The leading DM signature studied at colliders is the so-called mono-X channel where DM are usually produced at the primary collision vertex of the collider accompanied by a standard model (SM) particle X [5–9]. Over the years, a plethora of mono-X processes have been studied, with X being photon [5, 10–12], jet [6–8, 13–15], top [16–18], bottom [19, 20], Z/W [9, 21–26], or Higgs [27–31].

In this paper, we propose a new channel to search for DM at colliders where DM are produced in collisions between SM particles and the detector, instead of at the primary collision vertex of the collider. For concreteness, in this analysis we take as an example the Belle II experiment, the electron-positron collider operated at SuperKEKB. Belle II is expected to accumulate at least 50 ab^{-1} data and has a hermetic electromagnetic calorimeter

(ECL) [32], making it an ideal machine to search for light DM as well as other new light particles [33–47].

Electrons and positrons are copiously produced at Belle II via the Bhabha scattering process, leading to $\mathcal{O}(10^{12})$ positrons expected with 50 ab^{-1} . These final state positrons can then interact with the ECL detector to produce DM, as shown in Fig. (1). The interactions between the positron and the ECL can occur either via annihilations with atomic electrons in the ECL (the annihilation process)

$$e^+ + e_A^- \rightarrow \bar{\chi} + \chi, \quad (1.1)$$

or via scatterings with target nuclei in the ECL (the bremsstrahlung process)

$$e^+ + N \rightarrow e^+ + N + \bar{\chi} + \chi, \quad (1.2)$$

where χ is the DM particle, e_A^- is the atomic electron in the ECL, and N is the target nucleus, which can be either Cs or I in the ECL. The Feynman diagrams of these two processes are shown in Fig. (2). The DM particles then escape the Belle II detectors, resulting in a missing energy signature. We note that this channel is analogous to that in electron fixed-target experiments (e.g., NA64 [48]), with the ECL detector as the target.

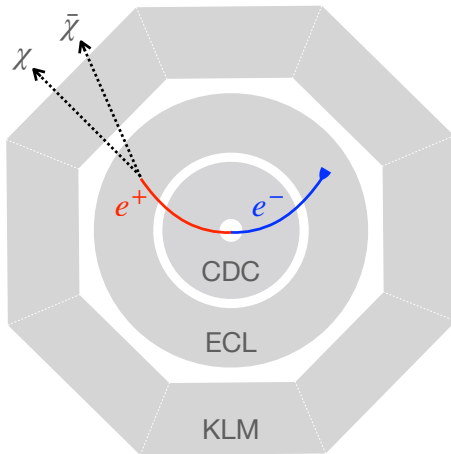


Figure 1. Schematic view of the signal event in the “disappearing positron track” channel, in the transverse plane of the Belle II detector.

Unlike DM produced at the primary collision vertex, the missing energy in this new channel is preceded by a charged track in the central drift chamber (CDC) and a small amount of energy deposited in the ECL. We thus refer to this new channel as the “disappearing positron track” channel.¹ Moreover, the disappearing positron is accompanied by an electron that has an opposite momentum to the positron track in the center of mass

¹We note that disappearing tracks have been searched for at the LHC in new physics studies; see e.g., Refs. [49, 50]. However, to our knowledge, the mechanism that leads to the disappearing track in this analysis has not been studied before. Moreover, the signature presented in this analysis has a unique event topology, which is distinct from various LHC studies.

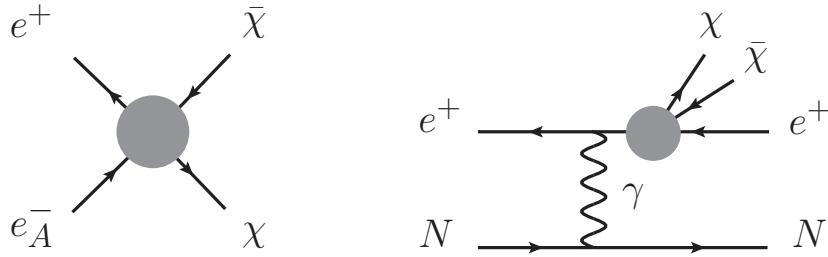


Figure 2. Feynman diagrams of the annihilation process $e^+e_A^- \rightarrow \bar{\chi}\chi$ (left), and the bremsstrahlung process $e^+N \rightarrow e^+N\bar{\chi}\chi$ (right). The process with $\bar{\chi}\chi$ radiated from the initial state e^+ is included in the analysis, but not shown here.

(c.m.) frame, a clear CDC track, and an energy deposition in the ECL that is consistent with the Bhabha scattering.

The collisions between positrons and the ECL can also produce photons and neutrons, which have a non-zero probability to penetrate all the sub-detectors of Belle II without leaving a trace, mimicking the signal events of DM. We find that a large missing energy in the ECL and a veto on a cluster or a track in the KLM (K_L -muon detector) [32, 46] are instrumental in controlling these backgrounds.

To illustrate the capability of this new channel in probing DM, we consider the dark photon (DP) model in which the DP predominantly decays into DM. The main results are summarized in Fig. (3). For the DP mass in the vicinity of 66 MeV, the new channel can probe unexplored parameter space, surpassing both the mono-photon channel at Belle II and the NA64 experiment. We note that, despite our efforts to reproduce the Belle II conditions to the best of our ability, the limits presented in this analysis should be revised by Belle II physicists using a full simulation of the detectors and inputs from data control samples. In particular, the various efficiency factors associated with the ECL and KLM detectors, which play a pivotal role in estimating the background, will be updated with a better understanding as the experiment progresses.

This rest of the paper is organized as follows. In section 2, we discuss the “disappearing positron track” signature at Belle II. In section 3, we discuss various SM backgrounds for the new signature. In section 4, we compute the signal events in the new channel for the invisible dark photon model, and further compare its sensitivity to other experimental searches, including the mono-photon channel at Belle II and the missing energy channel at NA64. In section 5, we summarize our findings. In the appendix, we provide the positron track length distribution for completeness, explore the dependence of the signal on the coupling constant, present our calculations on the NA64 constraints, discuss the backgrounds due to charged particles, compute the sensitivity on the scalar mediator model, and explore the sensitivity of the radiative Bhabha process.

2 Disappearing positron track

The energy of the final state positron is measured by the ECL detector, which has a barrel region and two endcap regions. In our analysis, we only consider the positrons in the barrel

region (with a polar angle between 32.2° and 128.7° in the lab frame), due to the following three reasons. First, there are less non-instrumented setups, such as magnetic wires and pole tips, between ECL and KLM in the barrel region as compared to the endcap regions [51]. This leads to a better KLM veto efficiency in the barrel region, which is essential in controlling the SM background. Second, the barrel region has a better hermiticity: Gaps between ECL crystals in the barrel region are non-projective to the collision point; however, some gaps in the endcap regions are projective so that particles can escape the ECL detector without being noticed when traversing them [52, 53]. Third, the endcap regions have more beam backgrounds [54].

Although in the signal process the positron cannot deposit all its energy in the ECL due to the production of DM, its transverse momentum can be measured in the CDC with a good resolution, e.g., $\delta p_T/p_T \simeq 0.4\%$ for $p_T \simeq 3$ GeV [55]. Using the CDC measurements (both the transverse momentum and the angular information), we can compute the positron energy, which is then required to be equal to the electron energy (measured both in the ECL and CDC) in the c.m. frame. To suppress the backgrounds (especially those from neutrons), we further require a large missing energy such that the final state positron only deposits at most 5% of its energy in the ECL, and veto KLM activities including multi-hits or a cluster.

We next compute the event number of positrons. Positrons at Belle II are mainly produced at the primary interaction point, via the Bhabha scattering process with the cross section [56]

$$\frac{d\sigma_B}{d\cos\theta^*} = \frac{\pi\alpha^2 (3 + \cos^2\theta^*)^2}{2s (1 + \cos\theta^*)^2}, \quad (2.1)$$

where θ^* is the polar angle of the final state positron in the c.m. frame, s is the square of the center of mass energy, and $\alpha \simeq 1/137$ is the fine structure constant. Because SuperKEKB is an asymmetric collider, which collides 7 GeV electrons with 4 GeV positrons [32], the differential cross section of the Bhabha scattering in the lab frame is given by

$$\frac{d\sigma_B}{dE} = \frac{d\sigma_B}{d\cos\theta^*} \frac{\sqrt{1-\beta^2}}{\beta E^*}, \quad (2.2)$$

where E is the energy of the final state positron in the lab frame, $\beta = 3/11$, $E^* = \sqrt{s}/2$, and $\cos\theta^* = (\sqrt{1-\beta^2}E/E^* - 1)/\beta$. In the lab frame, the energy of the final state positron E is related to its polar angle θ via $E = E^* \sqrt{1-\beta^2}/(1-\beta\cos\theta)$. Thus, the minimum and maximum energy of the positron at the barrel region in the lab frame are $E_{\min} \simeq 4.35$ GeV (for $\theta = 128.7^\circ$) and $E_{\max} \simeq 6.62$ GeV (for $\theta = 32.2^\circ$) respectively. The total number of positrons in the barrel region is about 6×10^{11} with the total luminosity of 50 ab^{-1} .

3 Standard Model Backgrounds

SM backgrounds arise when the SM particles that are produced in the collision between the final state positron and the ECL detector escape detection. Charged particles (such as electron and muon) are likely to be detected by the ECL and KLM detectors: The probability for positrons to penetrate the ECL is very small; the KLM detector, which consists

of an alternating sandwich of 4.7 cm thick iron plates and active detector elements [32], is very sensitive to the muon tracks, leading to negligible muon backgrounds via the KLM veto.² On the other hand, neutral particles (such as photon, neutron, and neutrino) have a significant probability to traverse the ECL and KLM detectors without being detected. Backgrounds due to neutrinos are found to be negligible, due to the large W/Z masses. Thus, the main backgrounds are due to photons and neutrons, which we discuss below.

3.1 Photon-induced backgrounds

We first discuss the photon-induced backgrounds. Photon energy can be measured in the ECL detector, which is made up of CsI crystals with the length of $16 X_0$ [57], where $X_0 = 1.86$ cm is the radiation length of CsI [58]. The energy distribution of photons that are produced in the collision between a positron with energy E and the ECL can be well approximated by [59]

$$\frac{dN_\gamma}{dx_\gamma}(t, x_\gamma) \simeq \frac{1}{x_\gamma} \frac{(1 - x_\gamma)^{(4/3)t} - e^{-(7/9)t}}{7/9 + (4/3) \ln(1 - x_\gamma)}, \quad (3.1)$$

where $x_\gamma = E_\gamma/E$ with E_γ being the energy of the photon, and tX_0 is the position of the photon in the ECL detector. Therefore, the probability of a photon carrying more than 95% of the positron energy to escape the ECL detector is given by³

$$\int_{0.95}^1 dx_\gamma \frac{dN_\gamma}{dx_\gamma}(t = 16, x_\gamma) \simeq 4.7 \times 10^{-8}. \quad (3.2)$$

This leads to $\sim 2.8 \times 10^4$ potential background events after the ECL detector, for the 6×10^{11} positrons. Although the probability for GeV-scale photons to penetrate the whole KLM (consisting of at least 60 cm iron plates in total [32]) without producing KLM clusters is negligibly small, photons can also be absorbed by some non-instrumented setups (for example the magnet coil) between the ECL and the KLM [51]. For that reason the veto power of the KLM on photons is limited. To take into account such effects, we adopt the IFR veto efficiency at BABAR, which is about 4.5×10^{-4} in the barrel region [61], as the conservative estimate of the KLM veto efficiency, since the KLM veto efficiency is expected to be better than the IFR [62].⁴ This then leads to 13 background events due to photons, for the 6×10^{11} positrons. We note that a small fraction of secondary photons can leak into the endcap region, where the veto efficiency is somewhat reduced; in our analysis, we have neglected this small effect. We also note that if the KLM veto efficiency can be improved by one order of magnitude as compared to the IFR, the photon backgrounds will decrease to be about a single event. On the other hand, if the KLM veto efficiency

²See appendix D for more detailed discussions on backgrounds due to charged particles.

³The analytic method is able to yield very accurate results. For example, by using the NA64 parameters, we find that Eq. (3.2) gives consistent results on the photon background with GEANT4 simulations in Ref. [60].

⁴We note that the term ‘‘veto efficiency’’ represents the probability that the intended events do not satisfy the veto conditions. Thus, the ‘‘veto efficiency’’ actually describes the inefficiency of the veto. In other words, a smaller value of the veto efficiency means a better veto (on the intended events).

turns out to be inferior to that of the IFR, an increase in photon-induced background events is expected. To account for this possibility, in section 4, we compute the Belle II sensitivity both with the background events analyzed in our current analysis and with a more conservative background level. The sensitivities under these different background assumptions are given in Fig. (3).

3.2 Neutron-induced backgrounds

We next discuss the neutron-induced backgrounds. Neutrons with energy of several GeV are mainly produced by photo-nuclear reactions between the positron and the ECL detector [58]. To estimate such backgrounds, we simulate collisions of 10^9 positrons with 4.35 GeV energy onto a CsI target with one X_0 , by using GEANT4 (version 11.0) [63] with the FTTP_BERT physics list. Our choice of the positron energy in the simulation is motivated by the fact that $\sim 50\%$ of the positrons are in the first tenth of the entire energy range in the barrel region, according to Eq. (2.2). We only simulate a fraction of positrons with a thin CsI target (with one X_0) because the full simulation with a $16\text{-}X_0$ CsI target is extremely time-consuming. The simulation results with the thin CsI target are acceptable for our purpose, because neutrons with significant energy are mainly produced within the first radiation length, which are confirmed in our simulations with a $2\text{-}X_0$ CsI target.

To ensure that the missing energy is mainly caused by neutrons, we only select the GEANT4 simulated events that contain at least one neutron with energy exceeding 3 GeV. There are 4950 events in the 10^9 simulations that satisfy this selection cut. We then compute the total energy deposited in the ECL, by taking into account both the deposited energy in the first X_0 calculated by GEANT4, and the kinetic energy of e^\pm and γ . We further include the kinetic energy of protons with momentum less than 0.6 GeV, because such protons have a gyroradius radius $\lesssim 1.3$ m in the ECL where $B = 1.5$ T [32], and thus can deposit the kinetic energy when orbiting around. We do not add the kinetic energy of π^\pm to the deposited energy, because π^\pm decays primarily into a neutrino and a muon which deposit negligible energy to the ECL. We then require the deposited energy in the ECL to be less than 5% of the energy of the positron; there are 100 events after this detector cut. We further veto events that contain protons or π^\pm with momentum exceeding 0.6 GeV, because these charged hadrons can either deposit significant energy in the ECL and/or produce tracks in the KLM. There are 64 events after this veto.

Next we classify the remaining events according to the number of neutrons that have kinetic energy exceeding 280 MeV, the energy threshold for hadronic showers [64]. There are 13 events with a single neutron and 51 events with more than 2 neutrons. We compute the probability for a neutron to penetrate a target with length L via [65, 66]

$$P = \exp(-L/\lambda_0), \quad (3.3)$$

where λ_0 is the hadronic interaction length. The KLM has $\sim 3.9\lambda_0$, and the ECL has $\sim 0.8\lambda_0$ [32]. We note that Eq. (3.3) can yield consistent results on neutron-induced backgrounds as compared with GEANT4 simulations in the context of the NA64 experiment [66]. Thus, the probability for a neutron to penetrate the remaining 15 X_0 's of the ECL

and the KLM is $P \simeq 0.01$.⁵ Rescaling this to the 6×10^{11} positrons, one expects ~ 81 background events due to neutrons in total.

We note that there is another source of neutrons from the beam backgrounds (dominated by 10-100 keV neutrons), which can also produce KLM hits [69] and thus complicates the situation. Because of the beam backgrounds, one cannot veto events with any hits in the KLM [51]. Fortunately, unlike neutrons with kinetic energy above 280 MeV which are expected to produce multi-hits or a cluster in the KLM, a single beam background neutron is usually absorbed in one scintillator strip [68]. For that reason, in our analysis, we only select neutrons above 280 MeV, which can be well controlled by the veto on multi-hits or a cluster in the KLM. However, since there is already a neutron with energy above 3 GeV in our selected events, including another neutron below 280 MeV would further suppress the background, leading to an even smaller neutron background. Thus, our analysis serves as a conservative estimate of the neutron backgrounds.

Taking into account backgrounds from both neutrons and photons, one expects at most ~ 94 background events for the 6×10^{11} positrons.

4 Sensitivity on dark matter in dark photon models

To show the sensitivity of the “disappearing positron track” channel on DM, we consider a new physics model in which DM interacts with the SM through a DP [70, 71]. In new physics scenarios where the SM gauge group is extended by an additional $U(1)$, DP can naturally arise, either via the kinetic mixing portal [72, 73], or via the Stueckelberg mass mixing portal [74–80]. For both portals, field redefinitions are necessary to recast the kinetic terms into canonical forms and to diagonalize the mass matrix for the neutral gauge bosons. These processes lead to DP interactions with matter fields both in the SM sector and in the dark sector. In the case of a small mixing parameter, the interaction Lagrangian can be parameterized as follows [71, 78]

$$\mathcal{L}_{\text{int}} = A'_\mu (eQ_f \epsilon \bar{f} \gamma^\mu f + g_\chi \bar{\chi} \gamma^\mu \chi), \quad (4.1)$$

where A'_μ is the DP with mass $m_{A'}$, χ is the Dirac DM with mass m_χ , f denotes the SM fermion with electric charge Q_f , ϵ is the small mixing parameter, e is the QED coupling constant, and g_χ is the hidden coupling constant. In our analysis we fix $m_\chi = m_{A'}/3$ such that A' decays dominantly into DM in the parameter space of interest where $g_\chi \gg e\epsilon$.

We compute the signal events from both diagrams shown in Fig. (2). We first compute the annihilation process $e^+e^- \rightarrow A' \rightarrow \chi\bar{\chi}$; the cross section is given by

$$\sigma_{\text{ann}}(\sqrt{s}) = \frac{e^2 \epsilon^2 \alpha_D}{3} \frac{s + 2m_\chi^2}{(s - m_{A'}^2)^2 + \Gamma_{A'}^2 m_{A'}^2} \sqrt{1 - \frac{4m_\chi^2}{s}}, \quad (4.2)$$

where $\alpha_D = g_\chi^2/4\pi$, $\Gamma_{A'}$ is the decay width of the DP, and $s = 2m_e E' + 2m_e^2 = 2m_e E_{A'}$ with E' being the energy of the positron at the collision point and $E_{A'} = E' + m_e$ being

⁵See e.g., Refs. [67, 68] for more detailed analyses on the role of the KLM detector as a hadronic veto.

the energy of A' . Note that we have $E' \leq E$ where E is the positron energy before entering ECL. The partial decay width of the DP into DM is

$$\Gamma(A' \rightarrow \bar{\chi}\chi) = \frac{m_{A'}\alpha_D}{3} \left(1 + 2\frac{m_\chi^2}{m_{A'}^2}\right) \sqrt{1 - \frac{4m_\chi^2}{m_{A'}^2}}. \quad (4.3)$$

Because the invisible decay width is much larger than the visible ones in the parameter space of interest, we use $\Gamma_{A'} \simeq \Gamma(A' \rightarrow \bar{\chi}\chi)$ in our analysis. The signal events in the annihilation process can be computed by [48, 81, 82]

$$N_{\text{ann}} = \mathcal{L} \int_{E_{\text{min}}}^{E_{\text{max}}} dE \frac{d\sigma_B}{dE} \int_{0.95E}^{E+m_e} dE_{A'} n_e T_e(E' = E_{A'} - m_e, E, L_T) \sigma_{\text{ann}}(E_{A'}), \quad (4.4)$$

where $\mathcal{L} = 50 \text{ ab}^{-1}$ is the integrated luminosity, n_e is the number density of the electron in CsI, and $d\sigma_B/dE$ is given in Eq. (2.2). Here $T_e(E', E, L_T)$ is the positron differential track-length distribution [59, 82–84] where $L_T = 16X_0$ is the thickness of the ECL target. The expression of T_e is given in appendix A. The integration of $E_{A'}$ is performed for $E_{A'} > 0.95E$ so that the positron deposits less than 5% of its original energy in the ECL.

We next compute the bremsstrahlung process. In the parameter space of interest, the signal is dominated by the on-shell produced A' . Thus, the signal events are given by

$$N_{\text{bre}} = \mathcal{L} \int_{E_{\text{min}}}^{E_{\text{max}}} dE \frac{d\sigma_B}{dE} \int_{0.95E}^{E-m_e} dE_{A'} \int_{E_{A'}}^E dE' n_N T_e(E', E, X_0) \frac{d\sigma_{\text{bre}}}{dE_{A'}}, \quad (4.5)$$

where n_N is the number density of I (or Cs). Here $d\sigma_{\text{bre}}/dE_{A'}$ are the differential cross section of the on-shell produced A' [85–88],

$$\frac{d\sigma_{\text{bre}}}{dE_{A'}} = (\phi_I + \phi_{\text{Cs}}) \frac{4\alpha^3 \epsilon^2}{E'} \frac{x(1-x+x^2/3)}{m_{A'}^2(1-x) + m_e^2 x^2}, \quad (4.6)$$

where $x \equiv E_{A'}/E'$, and ϕ_N denotes the effective flux of photons from nucleus N [85]:

$$\phi_N = \int_{t_{\text{min}}}^{t_{\text{max}}} dt \frac{t - t_{\text{min}}}{t^2} \left[\frac{Za^2 t}{(1+a^2 t)(1+t/d)} \right]^2, \quad (4.7)$$

with $t_{\text{min}} = (m_{A'}^2/2E')^2$, $t_{\text{max}} = m_{A'}^2 + m_e^2$, $a = 111m_e^{-1}Z^{-1/3}$, and $d = 0.164A^{-2/3} \text{ GeV}^2$. We use $Z = 53(55)$ and $A = 127(133)$ for I (Cs). Here we only consider the dominant elastic form factor.

Fig. (3) shows the expected 90% CL limits on the dark photon coupling parameter ϵ from the “disappearing positron track” channel, as a function of the DP mass, where we take $m_{A'} = 3m_\chi$, $\mathcal{L} = 50 \text{ ab}^{-1}$, and $\alpha_D = 0.001$. We compute the 90% CL limits by using $N_s/\sqrt{N_b} = \sqrt{2.71}$ [45] where $N_s = N_{\text{ann}} + N_{\text{bre}}$ and $N_b = 94$. We find that in the narrow mass window, $66 \text{ MeV} \lesssim m_{A'} \lesssim 82 \text{ MeV}$, the annihilation process with the atomic electrons dominates; outside this region, the bremsstrahlung process dominates. The narrow mass window can be explained by the Breit-Wigner resonance in Eq. (4.2), where one has $m_{A'} \simeq \sqrt{s} \simeq \sqrt{2E_e + m_e}$. The positron energy in the barrel region of the ECL

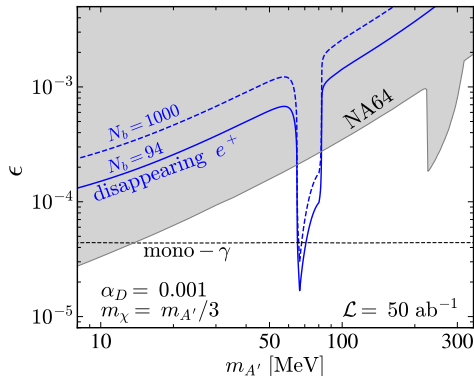


Figure 3. Belle II sensitivities on the coupling parameter ϵ between the DP and SM particles with 50 ab^{-1} integrated luminosity as a function of the DP mass $m_{A'}$ from the “disappearing positron track” with $N_b = 94$ (blue solid) and with $N_b = 1000$ (blue dashed). Here we fix $\alpha_D = 0.001$ and $m_\chi = m_{A'}/3$. Also shown are the Belle II sensitivity from the mono-photon channel with 50 ab^{-1} (black dashed), and the NA64 constraints (gray shaded region); see main text for details.

is in the range of 4.35-6.62 GeV, which leads to $66 \text{ MeV} \lesssim m_{A'} \lesssim 82 \text{ MeV}$ if the $< 5\%$ energy difference between secondary positrons and the incident positron is neglected. We thus refer to the narrow mass window where the annihilation process can proceed via the Breit-Wigner resonance of the mediator as the resonance region. The Belle II sensitivity in the resonance is significantly enhanced, as shown in Fig. (3).⁶

The DP models can also be searched for in the mono-photon channel $e^+e^- \rightarrow \gamma A'$ at Belle II [32] and by the missing energy signature at NA64 [48, 60]. The Belle II sensitivity from the mono-photon channel with 50 ab^{-1} , shown in Fig. (3), is rescaled from the result with 20 fb^{-1} in Ref. [32], assuming that the limit on ϵ is proportional to $\mathcal{L}^{-1/4}$.⁷ Fig. (3) shows the NA64 constraints with 2.84×10^{11} electrons on target in the $\alpha_D = 0.001$ case. The NA64 constraints away from the resonance region, which is $\sim (200 - 300) \text{ MeV}$, are from Ref. [60]. We compute the NA64 constraints in the resonance region by taking into account both the annihilation process and the bremsstrahlung process; the detailed calculations are given in appendix C, where we also carry out a comparison between our analytic method and the results given in Ref. [48], to demonstrate the accuracy of our calculation. For the $\alpha_D = 0.001$ case, if we take $N_b = 94$, we find that the best limit on ϵ from the new “disappearing positron track” channel is $\epsilon \lesssim 1.7 \times 10^{-5}$, which occurs in the vicinity of $m_{A'} \simeq 66 \text{ MeV}$, surpassing both the mono-photon channel at Belle II and the NA64 constraints. As α_D increases, the limits on ϵ are slightly weakened; for example, the best limit is $\epsilon \lesssim 2.6 \times 10^{-5}$ for the case of $\alpha_D = 0.1$. See appendix B for the detailed dependence

⁶We also anticipate such an enhancement for other mediators. In appendix E, we consider an alternative model where DM interacts with the SM sector via a scalar mediator. We find that the Belle II sensitivity on the scalar mediator model is similar to that of the dark photon model.

⁷Note that such a naive rescaling may not hold for the dark photon mass below 2 GeV, where the cosmic ray background becomes important and its characterization is yet to be completed [89]. Nevertheless, we provide such a rescaling of the mono-photon sensitivity as a comparison to our newly proposed channel.

of the limits on α_D .

In our benchmark model point, we have used the mass relation $m_{A'} = 3m_\chi$. We note that the limits have a weak dependence on m_χ , if it is decreased to even smaller values. For example, in the $m_{A'} = 66$ MeV case, the number of events is only decreased by $\sim 0.2\%$, if we change $m_{A'} = 3m_\chi$ to $m_{A'} = 5m_\chi$. This is because for the invisible dark photon model the signal process can be well approximated by the production of an on-shell dark photon.

We note that, despite our efforts to reproduce the Belle II conditions to the best of our ability, the photon- and neutron-induced backgrounds estimated in our analysis could still be subject to large uncertainties. To illustrate the impacts of these potential uncertainties on the sensitivity, we also compute the sensitivity with a background that is about one order of magnitude larger than our initial analysis. This is shown as the blue dashed curve with $N_b = 1000$ in Fig. (3). We find that the sensitivity on ϵ is weakened by a factor of $\simeq 1.8$, if the background is increased from $N_b = 94$ to $N_b = 1000$. This is because the new physics signal is proportional to ϵ^2 , while the expected limit on the new physics signal is proportional to $\sqrt{N_b}$. Even with $N_b = 1000$, we find that the sensitivity from the “disappearing positron track” in the resonance region, $66 \text{ MeV} \lesssim m_{A'} \lesssim 82 \text{ MeV}$, remains stronger than the NA64 constraint and can still be comparable to the mono-photon sensitivity from Belle II.

Here we discuss the possibility of using the “disappearing electron track” as a control sample. In this control sample, the electron in the final state of the Bhabha scattering interacts with the ECL to produce DM, with the positron being fully reconstructed. The control sample should yield a similar signal in the bremsstrahlung process as the “disappearing positron track”, but its signal in the annihilation process is very small. One might expect a null result in the annihilation process for the “disappearing electron track” because there are no atomic positrons in the ECL. However, secondary positrons can be generated when an electron traverses the ECL. By comparing the differential track lengths of positrons for incident electrons and positrons, which are given in Appendix A, we find that the secondary positrons that carry $> 95\%$ energy of the incident electron are smaller than those originating from an incident positron by a factor of $\sim 5 \times 10^{-4}$. Thus, the annihilation process in the control sample is expected to be smaller than the “disappearing positron track” by the same reduction factor. Because backgrounds are expected to be the same for both the “disappearing electron track” and the “disappearing positron track” channels, one can use the control sample to cross check the background analysis. The most interesting parameter space in our analysis occurs at $m_{A'} \simeq 66$ MeV and $2 \times 10^{-5} \lesssim \epsilon \lesssim 10^{-4}$, where the sensitivity is dominated by the annihilation between positrons and atomic electrons in the ECL. If excess events beyond the SM backgrounds were to be observed in this region for the “disappearing positron track”, one could cross check the signal with the control sample, which is expected to yield a signal that is a factor of $\sim 5 \times 10^{-4}$ smaller.

5 Conclusions

In this paper, we propose a new “disappearing positron track” channel at Belle II to search for DM, where DM are generated via collisions between positrons and the ECL. The major backgrounds are due to photons and neutrons produced in the same collisions. We design

a set of detector cuts to reconstruct such a new signal from the Belle II data, as well as to suppress various SM backgrounds. We compute the sensitivity of the new channel on the invisible dark photon model. We find that the new channel at Belle II can probe the dark photon coupling parameter $\epsilon \simeq 1.7 \times 10^{-5}$ with 50 ab^{-1} data for dark photon mass at $\sim 66.66 \text{ MeV}$, surpassing both the mono-photon channel at Belle II and the missing energy channel at NA64. We note that the disappearing track signal on positrons can be further extended to other SM particles at different particle colliders, thus presenting an opportunity to probe various new physics models with diverse interactions.

Acknowledgments

We thank Luigi Corona, Torben Ferber, and Li-Gang Xia for correspondence and discussions. We also would like to thank the anonymous referee for many valuable comments. The work is supported in part by the National Natural Science Foundation of China under Grant Nos. 12275128 and 12147103, by the Science and Technology Program of Guangzhou No. 2019050001, and by the Guangdong Major Project of Basic and Applied Basic Research No. 2020B0301030008.

A Track-length distribution of positrons and electrons

For an incident positron with an initial energy E to enter a target with thickness L_T , the differential track-length distribution of positrons as a function of the positron energy E' can be computed by [82, 84]

$$T_e(E', E, L_T) = X_0 \int_0^{L_T/X_0} I_e(E', E, t) dt, \quad (\text{A.1})$$

where X_0 is the radiation length of the target. Here $I_e(E', E, t)$ is the energy distribution of E' at the depth tX_0 , which can be computed iteratively such that $I_e = \sum_i I_e^{(i)}$ where $I_e^{(i)}$ denotes the i -th generation positrons [59]. We adopt the analytical model of Ref. [59] up to second-generation positrons, which are found to be in good agreement with simulations in Ref. [82]. The contributions from the first two generations are [59]

$$I_e^{(1)}(E', E, t) = \frac{1}{E} \frac{(\ln(1/v))^{b_1 t - 1}}{\Gamma(b_1 t)}, \quad (\text{A.2})$$

$$I_e^{(2)}(E', E, t) = \frac{2}{E} \int_v^1 \frac{dx}{x^2} \frac{1}{b_2 + b_1 \ln(1-x)} \times \left[\frac{(1-x)^{b_1 t} - (1-v/x)^{b_1 t}}{b_1 \ln[(x-x^2)/(x-v)]} + \frac{e^{-b_2 t} - (1-v/x)^{b_1 t}}{b_2 + b_1 \ln(1-v/x)} \right], \quad (\text{A.3})$$

where $b_1 = 4/3$, $b_2 = 7/9$, $v = E'/E$. We note that the analytical expression for the positron track length (with the first two generations) can yield consistent results with GEANT4 simulations; see e.g., figure 4 of Ref. [82] for the comparison in the case of an aluminum target.

Note that Eqs. (A.1, A.2, A.3) can also be used to compute the track length distribution of electrons with an incident electron. We compute the track length distribution of positrons (electrons) with an incident electron (positron) via

$$\bar{T}_e(E', E, L_T) = X_0 \int_0^{L_T/X_0} I_e^{(2)}(E', E, t) dt, \quad (\text{A.4})$$

where we have only used $I_e^{(2)}$. This is because $I_e^{(1)}$ describes the effects of bremsstrahlung, and $I_e^{(2)}$ subsequently describes the production of the electron and positron pair due to the emitted photon [59].

B Dependence of signal on α_D

Here we investigate the dependence of the dark photon constraint from the “disappearing positron track” channel at Belle II on the gauge coupling constant α_D in the hidden sector.

Dark photons can be produced either in the bremsstrahlung process or in the annihilation process. In the bremsstrahlung process, because dark photons are on-shell produced, the cross section does not depend on α_D . However, in the annihilation process, the cross section depends on α_D through the Breit-Wigner form of the dark photon propagator, since the hidden decay width of the dark photon is proportional to α_D . Fig. (4) shows the

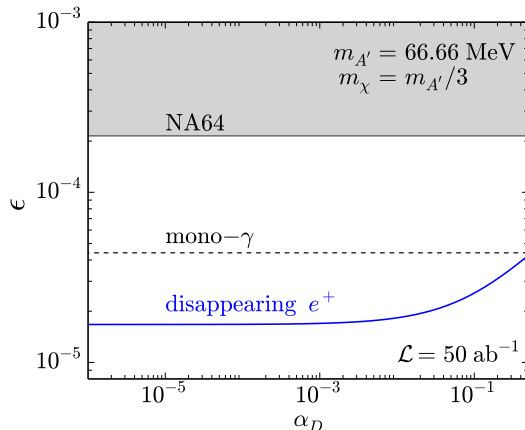


Figure 4. Belle II sensitivity on the coupling parameter ϵ with 50 ab^{-1} integrated luminosity as a function of α_D from the “disappearing positron track” (blue solid), where $m_{A'} = 66.66 \text{ MeV}$ and $m_\chi = m_{A'}/3$. The Belle II sensitivity from the mono-photon channel with 50 ab^{-1} (black dashed) is rescaled from the result with 20 fb^{-1} in Ref. [32]. The NA64 constraint with 2.84×10^{11} electrons on target (gray shaded region) is taken from Ref. [60].

constraints on the coupling parameter ϵ as a function of α_D , in which $m_{A'}$ is fixed to be 66.66 MeV . The upper bound on ϵ decreases with α_D until it saturates at $\epsilon \lesssim 1.7 \times 10^{-5}$ for $\alpha_D \lesssim 0.001$. Constraints from the missing energy signature at NA64 and from the mono-photon channel at Belle II are also shown in Fig. (4), which are independent of α_D . It is remarkable that the “disappearing positron track” channel for $\alpha_D \lesssim 0.5$ leads to a better

constraint than the mono-photon channel at Belle II and the missing energy signature at NA64.

C NA64 constraints

In this section, we compute the NA64 constraints. Note that Ref. [48] provided the NA64 constraints on dark photon with $\alpha_D = 0.1$ and $\alpha_D = 0.5$. In our calculation, we compute the NA64 constraints in the resonance region by taking into account the number of signal events both from the bremsstrahlung process (N_{bre}) and from the annihilation process (N_{ann}).

The NA64 constraint on the coupling parameter ϵ taking into account only the bremsstrahlung process (denoted as ϵ_{bre}) has been obtained in Ref. [60, 90], by requiring $N_s = 2.3$ where N_s is the number of signal events. Since the signal from the bremsstrahlung process is proportional to ϵ^2 and independent on α_D , we compute the number of signal events from the bremsstrahlung process via

$$N_{\text{bre}} = N_s \left(\frac{\epsilon^2}{\epsilon_{\text{bre}}^2} \right), \quad (\text{C.1})$$

where $N_s = 2.3$.

We compute the number of signal events from the annihilation process via

$$N_{\text{ann}} = \epsilon_d N_{\text{EOT}} \int_{0.5E}^{E+m_e} dE_{A'} \sigma_{\text{ann}}(E_{A'}) n_e T_e(E_{A'} - m_e, E, L_T), \quad (\text{C.2})$$

where $E = 100$ GeV is the energy of the incident electrons, $N_{\text{EOT}} = 2.84 \times 10^{11}$ is the number of electrons on target, n_e is the electron number density of the lead target, $\epsilon_d \simeq 0.5$ is the detection efficiency [60], σ_{ann} is the cross section of the annihilation process $e^- e^+ \rightarrow \chi \bar{\chi}$, $E_{A'}$ is the energy of the dark photon, L_T is the length of the target, and $T_e(E' = E_{A'} - m_e, E, L_T)$ is the positron differential track-length distribution.

We obtain the 90% C.L. constraints by using the criterion $N_{\text{ann}} + N_{\text{bre}} = 2.3$. We recompute the NA64 limits in Fig. (5) and compare them with those presented in the NA64 analysis [48], where GEANT4-based simulations are employed. As shown in Fig. (5), our calculation yields consistent results with Ref. [48]. In particular, in the vicinity of $m_{A'} \simeq 250$ MeV, where the $e^+ e^-$ annihilation process dominates, our analytic method utilizing Eq. (C.2) successfully reproduces the NA64 results [48], for both $\alpha_D = 0.5$ and $\alpha_D = 0.1$. This demonstrates the accuracy of our method, which utilizes the analytic expressions of the positron track length distribution (with the first two generations), in predicting dark photon signal events in the region dominated by the $e^+ e^-$ annihilation process.

D SM backgrounds due to charged particles

We have assumed in the analysis that charged particles lead to insubstantial backgrounds compared to neutral particles, such as photons and neutrons. Here, we provide a more detailed discussion of potential background sources due to charged particles.

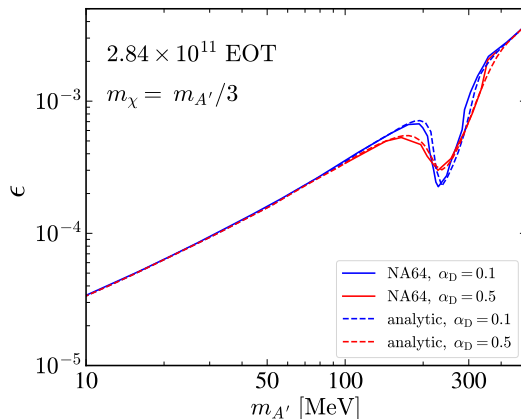


Figure 5. NA64 constraints (with 2.84×10^{11} electrons on target) obtained in our analytical calculations (dashed lines) and in Ref. [48] where GEANT4-based simulations are employed (solid lines). The comparison is carried out for the mass relation of $m_\chi = m_{A'}/3$ and for two different couplings: $\alpha_D = 0.1$ (blue) and $\alpha_D = 0.5$ (red).

Backgrounds can arise from pairs of charged particles generated in e^+e^- collisions at the primary vertex, with notable examples including $\pi^+\pi^-$ and $\mu^+\mu^-$. To be classified as a background contribution, the charged pair must satisfy the following criteria: The negatively charged particle within the pair must effectively mimic a fully reconstructed e^- , exhibiting successful reconstructions in both CDC and ECL (with nearly all of its energy deposited in ECL). Additionally, the positively charged particle should emulate a poorly reconstructed e^+ , featuring a robust reconstruction in CDC, but with less than 5% of its energy detected by ECL and no significant energy deposition in KLM (to avoid KLM veto).

We first discuss backgrounds due to the $\pi^+\pi^-$ final state generated in e^+e^- collisions at the primary vertex. First note that $\sigma(e^+e^- \rightarrow \pi^+\pi^-)$ at Belle II is significantly suppressed by the pion form factor, making it substantially smaller than leptonic final states, such as $\mu^+\mu^-$. We estimate $\sigma(e^+e^- \rightarrow \pi^+\pi^-)$ by utilizing the measurement of $d\sigma(\pi^+\pi^-)/dz$ in e^+e^- collisions conducted in Ref. [91], where $z = 2E_\pi/\sqrt{s}$ with $\sqrt{s} = 10.52$ GeV. To mimic the e^+e^- final state, z has to be close to 1. However, due to limitations of the method used in Ref. [91], $d\sigma(\pi^+\pi^-)/dz$ is provided only for $z < 0.98$. Since $d\sigma(\pi^+\pi^-)/dz$ decreases with increasing z , we take a conservative estimate by considering the measurement in the range of $0.95 < z < 0.98$; this gives $\sigma(e^+e^- \rightarrow \pi^+\pi^-) \simeq 0.3$ pb, thus leading to $\simeq 1.5 \times 10^7$ events for an integrated luminosity of 50 ab^{-1} at Belle II. Since we only consider the barrel region of the ECL, we adopt the mis-identification rate for π^- as e^- in the high p_T region, which is $\sim 3 \times 10^{-5}$ [92]. To determine the probability for a π^+ to deposit $< 5\%$ of its energy in the ECL, we carry out GEANT4 simulations and find that this probability is $\lesssim 10^{-5}$. Taking into account these two factors, backgrounds due to the $\pi^+\pi^-$ final state are $\simeq 4.5 \times 10^{-3}$. Thus, we expect that backgrounds due to a hadronic pair are negligible.

We next discuss backgrounds due to the $\mu^+\mu^-$ final state generated in e^+e^- collisions at the primary vertex, which has a production cross section of $\simeq 500$ pb at $\sqrt{s} = 10.58$ GeV

in the ECL barrel region, thus leading to $\simeq 2.5 \times 10^{10}$ events for an integrated luminosity of 50 ab^{-1} at Belle II. To determine the background, we carry out GEANT4 simulations for both μ^- and μ^+ in ECL. Because the energy resolution of ECL is $\delta E/E \simeq 2\%$ [32], we determine the probability for a μ^- to mimic an e^- in ECL by computing the probability for a μ^- to deposit $> 98\%$ of its energy in ECL; we find the probability to be $\lesssim 10^{-7}$ by using our GEANT4 simulations. We note that one of the processes in which a μ^- can mimic an e^- is one where μ^- emits a very hard and collinear radiation. The probability for a μ^+ to deposit $< 5\%$ of its energy in ECL is found to be $\simeq 90\%$. To estimate the KLM veto efficiency on the μ^+ , we adopt the KLM veto efficiency on photon, which is $\sim 4.5 \times 10^{-4}$ [61]. The backgrounds are reduced to a single event, after taking into account the above three factors. Given that KLM is a muon detector, we expect its veto efficiency for muons to surpass that for photons. Consequently, we anticipate that backgrounds due to $\mu^+\mu^-$ pairs will be negligible.

Backgrounds can also arise from the $e^+e^-e^+e^-$ final state, where a pair of e^+ and e^- is outside the acceptance of detectors. Another background can arise from the $\tau^+\tau^-$ final state, where τ^+ decays into $e^+/\mu^+/\pi^+$ and τ^- decays into e^- . However, due to energy carried away from the other particles, these two types of backgrounds do not exhibit the expected electron and positron momenta characteristic of Bhabha scattering events and can be effectively vetoed via track measurements in the CDC.

Another potential background arises when a pair of muons is produced in collisions between e^+ and the ECL, via the bremsstrahlung process: $e^+ + N \rightarrow e^+ + N + \mu^+ + \mu^-$, which has a cross section of $\sim 300 \text{ nb}$. This leads to ~ 3400 events with 6×10^{11} positrons hitting the ECL target. Once again, we adopt the KLM veto efficiency on photon as the efficiency on muon, which is $\sim 4.5 \times 10^{-4}$ [61]; applying this veto efficiency to both muons makes this type of background negligible.

E Sensitivity on the scalar mediator model

In this section we investigate the Belle II sensitivity on an alternative DM model from the “disappearing positron track” channel. Thus, we consider the scalar mediator model with the following interaction Lagrangian

$$\mathcal{L}_{\text{int}} = \phi(\epsilon \ell \bar{\ell} + g_\chi \bar{\chi} \chi), \quad (\text{E.1})$$

where ϕ is the scalar mediator with mass m_ϕ , and ℓ is the SM charged lepton. Similar to the invisible dark photon case, we assume $m_\chi = m_\phi/3$ and $g_\chi \gg \epsilon \ell$ such that ϕ decays dominantly into DM with the decay width

$$\Gamma_\phi = \frac{m_\phi \alpha_D}{2} \left(1 - 4 \frac{m_\chi^2}{m_\phi^2} \right) \sqrt{1 - \frac{4m_\chi^2}{m_\phi^2}}. \quad (\text{E.2})$$

We follow the same procedure in section 4 to compute the Belle II sensitivity on the scalar mediator model from the “disappearing positron track” channel, which is shown in Fig. (6). Similar to the invisible dark photon model, the sensitivity on the scalar mediator

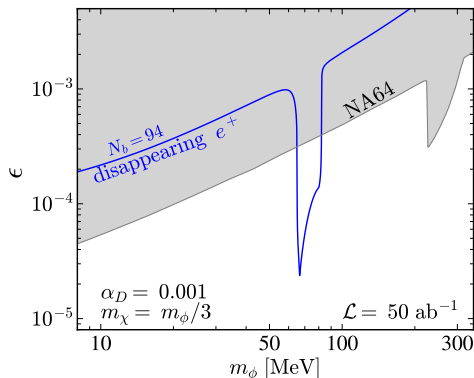


Figure 6. Belle II sensitivity on the coupling parameter ϵ as a function of the scalar mediator mass m_ϕ from the “disappearing positron track” with $N_b = 94$ and $\mathcal{L} = 50 \text{ ab}^{-1}$. Here we fix $\alpha_D = 0.001$ and $m_\chi = m_\phi/3$. For the NA64 constraint, we adopt the limits from Ref. [90] due to the bremsstrahlung process, and use the method in appendix C for the resonance region.

model is also significantly enhanced in the resonance region near $m_\phi = 66 \text{ MeV}$. The sensitivity in the resonance region is dominated by the annihilation process, $e^+e_A^- \rightarrow \phi \rightarrow \chi\bar{\chi}$, which has the following cross section:

$$\sigma_S = \frac{e^2\epsilon^2\alpha_D}{4} \frac{s - 4m_\chi^2}{(s - m_\phi^2)^2 + \Gamma_\phi^2 m_\phi^2} \sqrt{1 - \frac{4m_\chi^2}{s}}. \quad (\text{E.3})$$

The best limit on the coupling parameter in the resonance region is $\epsilon \simeq 2.4 \times 10^{-5}$, which is slightly weakened as compared to the dark photon case. We note that the change of the ϵ limit can be explained by the fact that in the narrow width approximation, the new physics signal is proportional to $(2J + 1)\Gamma(M \rightarrow e^+e^-)$, where J is the spin of the mediator M .

F Sensitivity of the radiative Bhabha scattering process

In this section we discuss the potential sensitivity of the “disappearing positron track” channel for positrons generated by the radiative Bhabha scattering (RBS) process, $e^+e^- \rightarrow e^+e^-\gamma$. Although the RBS cross section is expected to be smaller by a factor of $\alpha \simeq 1/137$ than that of the Bhabha scattering (BS) process, positrons from the RBS process exhibit a broader energy range, as shown in Fig. (7), which thus have the potential to probe different parameter space in the resonance region via the annihilation process.

As discussed in section 2, the missing energy in the positron track can be obtained by comparing the momentum of the positron inferred from the CDC track with the energy deposition in the ECL. In the BS events, the energy of the positron can be further cross-checked by its polar angle and the measurement of the electron. In contrast, there is no simple relation between the positron energy with its polar angle. But one can still reconstruct the energies and momenta of all the three final state particles and then use the momentum conservation to cross-check the measurement on the positron. Note that

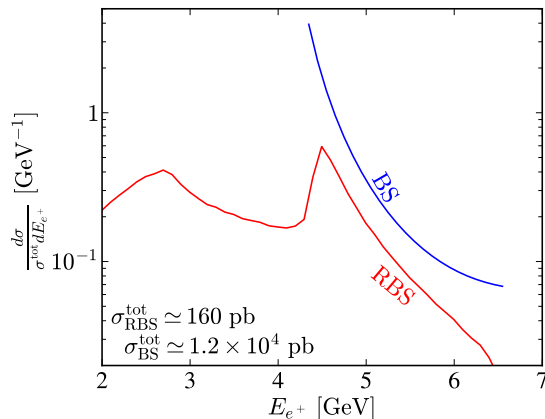


Figure 7. The normalized positron energy spectra of both the BS ($e^+e^- \rightarrow e^+e^-$) and the RBS ($e^+e^- \rightarrow e^+e^-\gamma$) processes, where $\sigma^{\text{tot}} \simeq 160$ (1.2×10^4) pb is the total cross section for the RBS (BS) case. The BS case is given by Eq. (2.2). The RBS case is obtained from MadGraph simulations, where all the three final state particles are required to be within the ECL barrel region and have energy above 2 GeV; moreover, the photon is required to have a angular distance $\Delta R > 0.1$ from both the electron and the positron.

the energy resolution of ECL is $\sigma_E/E = 1.6\%$ (4%) at 8 GeV (100 MeV), and the angular resolution of ECL at high (low) energies is 3 (13) mrad [32]. Thus the angular information of the photon can be well-measured by the ECL.

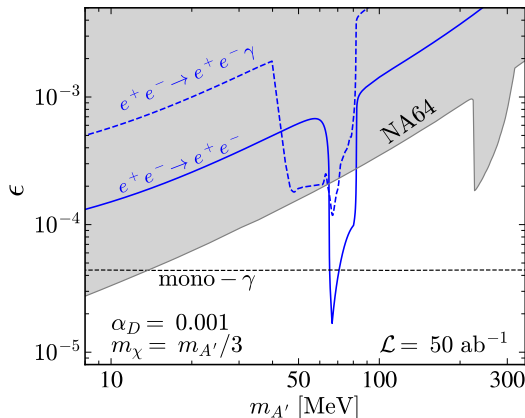


Figure 8. Belle II sensitivities on the coupling parameter ϵ with 50 ab^{-1} integrated luminosity as a function of the DP mass $m_{A'}$ from the “disappearing positron track” channel for the Bhabha scattering process with $N_b = 94$ (blue solid) and for the radiative Bhabha scattering process with $N_b = 1$ (blue dashed). Here we fix $\alpha_D = 0.001$ and $m_\chi = m_{A'}/3$. Also shown are the Belle II sensitivity from the mono-photon channel with 50 ab^{-1} (black dashed), and the NA64 constraints (gray shaded region).

To compute the cross section and the positron energy spectrum in the RBS process, we simulated 10^6 RBS ($e^+e^- \rightarrow e^+e^-\gamma$) events by using MADGRAPH [93]. In our simulation,

we require each of the three final state particles to have $E > 2$ GeV and $32.2^\circ < \theta < 128.7^\circ$ in the lab frame; we further require that the photon does not appear in the vicinity of both the electron and the positron such that the angular distance $\Delta R_{\gamma e^\pm}$ is greater than 0.1. Under these detector cuts, we find that the total cross section is $\simeq 160$ pb, corresponding to $\simeq 8 \times 10^9$ events with a luminosity of 50 ab^{-1} . To compute the number of the signal events in the invisible dark photon model, we use Eq. (4.4) and Eq. (4.5), where $d\sigma_B/dE$ is obtained by the RBS events in our simulation, as shown in Fig. (7). In section 3, we have found that there are $\simeq 94$ backgrounds due to punch-through neutrons/photons for the $\simeq 6 \times 10^{11}$ BS positrons in the ECL barrel region. Thus, one expect $\simeq 1$ background for the $\simeq 8 \times 10^9$ RBS events. Fig. (8) shows the 90% CL upper bound on ϵ from the RBS process, where the criterion of $N_s = 3$ is used. The resonance region for the RBS process expands to the range of $40 \text{ MeV} \lesssim m_{A'} \lesssim 80 \text{ MeV}$, due to the broader range of the positron energy. The limit improves within the mass range of $40 \text{ MeV} \lesssim m_{A'} \lesssim 60 \text{ MeV}$, reaching a level comparable to the NA64 constraints.

References

- [1] G. Bertone and D. Hooper, “History of dark matter,” *Rev. Mod. Phys.* **90** (2018) 045002 [[arXiv:1605.04909](#)].
- [2] J. Alexander *et al.*, “Dark Sectors 2016 Workshop: Community Report.” [arXiv:1608.08632](#).
- [3] M. Battaglieri *et al.*, “US Cosmic Visions: New Ideas in Dark Matter 2017: Community Report.” [arXiv:1707.04591](#).
- [4] A. Arbey and F. Mahmoudi, “Dark matter and the early Universe: a review,” *Prog. Part. Nucl. Phys.* **119** (2021) 103865 [[arXiv:2104.11488](#)].
- [5] A. Birkedal, K. Matchev, and M. Perelstein, “Dark matter at colliders: A Model independent approach,” *Phys. Rev. D* **70** (2004) 077701 [[hep-ph/0403004](#)].
- [6] J. L. Feng, S. Su, and F. Takayama, “Lower limit on dark matter production at the large hadron collider,” *Phys. Rev. Lett.* **96** (2006) 151802 [[hep-ph/0503117](#)].
- [7] M. Beltran, D. Hooper, E. W. Kolb, Z. A. C. Krusberg, and T. M. P. Tait, “Maverick dark matter at colliders,” *JHEP* **09** (2010) 037 [[arXiv:1002.4137](#)].
- [8] Y. Bai, P. J. Fox, and R. Harnik, “The Tevatron at the Frontier of Dark Matter Direct Detection,” *JHEP* **12** (2010) 048 [[arXiv:1005.3797](#)].
- [9] F. J. Petriello, S. Quackenbush, and K. M. Zurek, “The Invisible Z' at the CERN LHC,” *Phys. Rev. D* **77** (2008) 115020 [[arXiv:0803.4005](#)].
- [10] P. J. Fox, R. Harnik, J. Kopp, and Y. Tsai, “LEP Shines Light on Dark Matter,” *Phys. Rev. D* **84** (2011) 014028 [[arXiv:1103.0240](#)].
- [11] Y. Gershtein, F. Petriello, S. Quackenbush, and K. M. Zurek, “Discovering hidden sectors with mono-photon Z' searches,” *Phys. Rev. D* **78** (2008) 095002 [[arXiv:0809.2849](#)].
- [12] W. Abdallah, J. Fiaschi, S. Khalil, and S. Moretti, “Mono-jet, -photon and -Z signals of a supersymmetric (B – L) model at the Large Hadron Collider,” *JHEP* **02** (2016) 157 [[arXiv:1510.06475](#)].

- [13] P. J. Fox, R. Harnik, J. Kopp, and Y. Tsai, “Missing Energy Signatures of Dark Matter at the LHC,” *Phys. Rev. D* **85** (2012) 056011 [[arXiv:1109.4398](#)].
- [14] A. Rajaraman, W. Shepherd, T. M. P. Tait, and A. M. Wijangco, “LHC Bounds on Interactions of Dark Matter,” *Phys. Rev. D* **84** (2011) 095013 [[arXiv:1108.1196](#)].
- [15] M. Papucci, A. Vichi, and K. M. Zurek, “Monojet versus the rest of the world I: t-channel models,” *JHEP* **11** (2014) 024 [[arXiv:1402.2285](#)].
- [16] J. Andrea, B. Fuks, and F. Maltoni, “Monotops at the LHC,” *Phys. Rev. D* **84** (2011) 074025 [[arXiv:1106.6199](#)].
- [17] J.-L. Agram, J. Andrea, M. Buttignol, E. Conte, and B. Fuks, “Monotop phenomenology at the Large Hadron Collider,” *Phys. Rev. D* **89** (2014) 014028 [[arXiv:1311.6478](#)].
- [18] I. Boucheneb, G. Cacciapaglia, A. Deandrea, and B. Fuks, “Revisiting monotop production at the LHC,” *JHEP* **01** (2015) 017 [[arXiv:1407.7529](#)].
- [19] T. Lin, E. W. Kolb, and L.-T. Wang, “Probing dark matter couplings to top and bottom quarks at the LHC,” *Phys. Rev. D* **88** (2013) 063510 [[arXiv:1303.6638](#)].
- [20] E. Izaguirre, G. Krnjaic, and B. Shuve, “The Galactic Center Excess from the Bottom Up,” *Phys. Rev. D* **90** (2014) 055002 [[arXiv:1404.2018](#)].
- [21] L. M. Carpenter, A. Nelson, C. Shimmin, T. M. P. Tait, and D. Whiteson, “Collider searches for dark matter in events with a Z boson and missing energy,” *Phys. Rev. D* **87** (2013) 074005 [[arXiv:1212.3352](#)].
- [22] N. F. Bell, *et al.*, “Searching for Dark Matter at the LHC with a Mono-Z,” *Phys. Rev. D* **86** (2012) 096011 [[arXiv:1209.0231](#)].
- [23] N. F. Bell, Y. Cai, and R. K. Leane, “Mono-W Dark Matter Signals at the LHC: Simplified Model Analysis,” *JCAP* **01** (2016) 051 [[arXiv:1512.00476](#)].
- [24] N. F. Bell, Y. Cai, J. B. Dent, R. K. Leane, and T. J. Weiler, “Dark matter at the LHC: Effective field theories and gauge invariance,” *Phys. Rev. D* **92** (2015) 053008 [[arXiv:1503.07874](#)].
- [25] U. Haisch, F. Kahlhoefer, and T. M. P. Tait, “On Mono-W Signatures in Spin-1 Simplified Models,” *Phys. Lett. B* **760** (2016) 207–213 [[arXiv:1603.01267](#)].
- [26] Y. Bai and T. M. P. Tait, “Searches with Mono-Leptons,” *Phys. Lett. B* **723** (2013) 384–387 [[arXiv:1208.4361](#)].
- [27] A. A. Petrov and W. Shepherd, “Searching for dark matter at LHC with Mono-Higgs production,” *Phys. Lett. B* **730** (2014) 178–183 [[arXiv:1311.1511](#)].
- [28] L. Carpenter, *et al.*, “Mono-Higgs-boson: A new collider probe of dark matter,” *Phys. Rev. D* **89** (2014) 075017 [[arXiv:1312.2592](#)].
- [29] A. Berlin, T. Lin, and L.-T. Wang, “Mono-Higgs Detection of Dark Matter at the LHC,” *JHEP* **06** (2014) 078 [[arXiv:1402.7074](#)].
- [30] K. Ghorbani and L. Khalkhali, “Mono-Higgs signature in a fermionic dark matter model,” *J. Phys. G* **44** (2017) 105004 [[arXiv:1608.04559](#)].
- [31] J. M. No, “Looking through the pseudoscalar portal into dark matter: Novel mono-Higgs and mono-Z signatures at the LHC,” *Phys. Rev. D* **93** (2016) 031701 [[arXiv:1509.01110](#)].

- [32] E. Kou and P. Urquijo, eds., “The Belle II Physics Book,” *PTEP* **2019** (2019) 123C01 [[arXiv:1808.10567](#)]. [Erratum: *PTEP* 2020, 029201 (2020)].
- [33] T. Hauth, “Search for dark matter and dark sector at Belle II,” *PoS HQL2018* (2018) 060.
- [34] J. Liang, Z. Liu, Y. Ma, and Y. Zhang, “Millicharged particles at electron colliders,” *Phys. Rev. D* **102** (2020) 015002 [[arXiv:1909.06847](#)].
- [35] T. Araki, S. Hoshino, T. Ota, J. Sato, and T. Shimomura, “Detecting the $L_\mu - L_\tau$ gauge boson at Belle II,” *Phys. Rev. D* **95** (2017) 055006 [[arXiv:1702.01497](#)].
- [36] Y. Zhang, *et al.*, “Probing the $L_\mu - L_\tau$ gauge boson at electron colliders,” *Phys. Rev. D* **103** (2021) 015008 [[arXiv:2012.10893](#)].
- [37] D. W. Kang, P. Ko, and C.-T. Lu, “Exploring properties of long-lived particles in inelastic dark matter models at Belle II,” *JHEP* **04** (2021) 269 [[arXiv:2101.02503](#)].
- [38] M. Duerr, *et al.*, “Invisible and displaced dark matter signatures at Belle II,” *JHEP* **02** (2020) 039 [[arXiv:1911.03176](#)].
- [39] M. Duerr, T. Ferber, C. Garcia-Cely, C. Hearty, and K. Schmidt-Hoberg, “Long-lived Dark Higgs and Inelastic Dark Matter at Belle II,” *JHEP* **04** (2021) 146 [[arXiv:2012.08595](#)].
- [40] T. Ferber, C. Garcia-Cely, and K. Schmidt-Hoberg, “Belle II sensitivity to long-lived dark photons.” [arXiv:2202.03452](#).
- [41] **Belle-II** Collaboration, “Search for Axion-Like Particles produced in e^+e^- collisions at Belle II,” *Phys. Rev. Lett.* **125** (2020) 161806 [[arXiv:2007.13071](#)].
- [42] E. Izaguirre, T. Lin, and B. Shuve, “Searching for Axionlike Particles in Flavor-Changing Neutral Current Processes,” *Phys. Rev. Lett.* **118** (2017) 111802 [[arXiv:1611.09355](#)].
- [43] Y. Jho, Y. Kwon, S. C. Park, and P.-Y. Tseng, “Search for muon-philic new light gauge boson at Belle II,” *JHEP* **10** (2019) 168 [[arXiv:1904.13053](#)].
- [44] **Belle-II** Collaboration, “Search for an Invisibly Decaying Z' Boson at Belle II in $e^+e^- \rightarrow \mu^+\mu^-(e^\pm\mu^\mp)$ Plus Missing Energy Final States,” *Phys. Rev. Lett.* **124** (2020) 141801 [[arXiv:1912.11276](#)].
- [45] J. Liang, Z. Liu, and L. Yang, “Probing sub-GeV leptophilic dark matter at Belle II and NA64,” *JHEP* **05** (2022) 184 [[arXiv:2111.15533](#)].
- [46] M. J. Dolan, T. Ferber, C. Hearty, F. Kahlhoefer, and K. Schmidt-Hoberg, “Revised constraints and Belle II sensitivity for visible and invisible axion-like particles,” *JHEP* **12** (2017) 094 [[arXiv:1709.00009](#)]. [Erratum: *JHEP* 03, 190 (2021)].
- [47] T. Bandyopadhyay, S. Chakraborty, and S. Trifinopoulos, “Displaced searches for light vector bosons at Belle II,” *JHEP* **05** (2022) 141 [[arXiv:2203.03280](#)].
- [48] Y. M. Andreev *et al.*, “Improved exclusion limit for light dark matter from e^+e^- annihilation in NA64,” *Phys. Rev. D* **104** (2021) L091701 [[arXiv:2108.04195](#)].
- [49] **ATLAS** Collaboration, “Search for long-lived charginos based on a disappearing-track signature using 136 fb^{-1} of pp collisions at $\sqrt{s} = 13 \text{ TeV}$ with the ATLAS detector,” *Eur. Phys. J. C* **82** (2022) 606 [[arXiv:2201.02472](#)].
- [50] **CMS** Collaboration, “Search for supersymmetry in final states with disappearing tracks in proton-proton collisions at $\sqrt{s} = 13 \text{ TeV}$.” [arXiv:2309.16823](#).
- [51] Torben Ferber, private communication.

- [52] C. Hearty. https://indico.fnal.gov/event/13702/contributions/21158/attachments/13740/17506/Dark_sector_BaBar_Belle_II_Hearty.pdf.
- [53] Belle Collaboration, “The Belle Detector,” *Nucl. Instrum. Meth. A* **479** (2002) 117–232.
- [54] S. R. de Jong, *Study of Thermal Neutron Flux from SuperKEKB in the Belle II Commissioning Detector*. PhD thesis, Victoria U., 2017.
- [55] T. V. Dong, *et al.*, “Calibration and alignment of the Belle II central drift chamber,” *Nucl. Instrum. Meth. A* **930** (2019) 132–141.
- [56] M. E. Peskin and D. V. Schroeder, *An Introduction to quantum field theory*. Addison-Wesley, Reading, USA, 1995.
- [57] **BELLE II calorimeter Group** Collaboration, “Electromagnetic calorimeter of the Belle II detector,” *J. Phys. Conf. Ser.* **928** (2017) 012021.
- [58] **Particle Data Group** Collaboration, “Review of Particle Physics,” *Phys. Rev. D* **98** (2018) 030001.
- [59] Y.-S. Tsai and V. Whitis, “THICK TARGET BREMSSTRAHLUNG AND TARGET CONSIDERATION FOR SECONDARY PARTICLE PRODUCTION BY ELECTRONS,” *Phys. Rev.* **149** (1966) 1248–1257.
- [60] D. Banerjee *et al.*, “Dark matter search in missing energy events with NA64,” *Phys. Rev. Lett.* **123** (2019) 121801 [[arXiv:1906.00176](https://arxiv.org/abs/1906.00176)].
- [61] **BaBar** Collaboration in *34th International Conference on High Energy Physics*. 2008. [arXiv:0808.0017](https://arxiv.org/abs/0808.0017).
- [62] Luigi Corona, private communication.
- [63] **GEANT4** Collaboration, “GEANT4—a simulation toolkit,” *Nucl. Instrum. Meth. A* **506** (2003) 250–303.
- [64] L. Cerrito, *Radiation and Detectors: Introduction to the Physics of Radiation and Detection Devices*. Graduate Texts in Physics. Springer, 2017.
- [65] C. Grupen and B. Schwartz, *Particle detectors*. Cambridge Univ. Pr., Cambridge, UK, 2008.
- [66] S. Andreas *et al.*, “Proposal for an Experiment to Search for Light Dark Matter at the SPS.” [arXiv:1312.3309](https://arxiv.org/abs/1312.3309).
- [67] Belle Collaboration, “Search for $B^0 \rightarrow \pi^- \tau^+ \nu_\tau$ with hadronic tagging at Belle,” *Phys. Rev. D* **93** (2016) 032007 [[arXiv:1509.06521](https://arxiv.org/abs/1509.06521)].
- [68] T. Aushev *et al.*, “A scintillator based endcap K_L and muon detector for the Belle II experiment,” *Nucl. Instrum. Meth. A* **789** (2015) 134–142 [[arXiv:1406.3267](https://arxiv.org/abs/1406.3267)].
- [69] **Belle-II** Collaboration, “Belle II Technical Design Report.” [arXiv:1011.0352](https://arxiv.org/abs/1011.0352).
- [70] J. Jaeckel and A. Ringwald, “The Low-Energy Frontier of Particle Physics,” *Ann. Rev. Nucl. Part. Sci.* **60** (2010) 405–437 [[arXiv:1002.0329](https://arxiv.org/abs/1002.0329)].
- [71] M. Fabbrichesi, E. Gabrielli, and G. Lanfranchi, “The Dark Photon.” [arXiv:2005.01515](https://arxiv.org/abs/2005.01515).
- [72] B. Holdom, “Two U(1)’s and Epsilon Charge Shifts,” *Phys. Lett. B* **166** (1986) 196–198.
- [73] R. Foot and X.-G. He, “Comment on Z Z-prime mixing in extended gauge theories,” *Phys. Lett. B* **267** (1991) 509–512.

- [74] B. Kors and P. Nath, “Aspects of the Stueckelberg extension,” *JHEP* **07** (2005) 069 [[hep-ph/0503208](#)].
- [75] D. Feldman, Z. Liu, and P. Nath, “Probing a very narrow Z-prime boson with CDF and D0 data,” *Phys. Rev. Lett.* **97** (2006) 021801 [[hep-ph/0603039](#)].
- [76] D. Feldman, Z. Liu, and P. Nath, “The Stueckelberg Z Prime at the LHC: Discovery Potential, Signature Spaces and Model Discrimination,” *JHEP* **11** (2006) 007 [[hep-ph/0606294](#)].
- [77] K. Cheung and T.-C. Yuan, “Hidden fermion as milli-charged dark matter in Stueckelberg Z-prime model,” *JHEP* **03** (2007) 120 [[hep-ph/0701107](#)].
- [78] D. Feldman, Z. Liu, and P. Nath, “The Stueckelberg Z-prime Extension with Kinetic Mixing and Milli-Charged Dark Matter From the Hidden Sector,” *Phys. Rev. D* **75** (2007) 115001 [[hep-ph/0702123](#)].
- [79] M. Du, Z. Liu, and V. Q. Tran, “Enhanced Long-Lived Dark Photon Signals at the LHC,” *JHEP* **05** (2020) 055 [[arXiv:1912.00422](#)].
- [80] M. Du, R. Fang, Z. Liu, and V. Q. Tran, “Enhanced long-lived dark photon signals at lifetime frontier detectors,” *Phys. Rev. D* **105** (2022) 055012 [[arXiv:2111.15503](#)].
- [81] S. N. Gninenko, D. V. Kirpichnikov, and N. V. Krasnikov, “Probing millicharged particles with NA64 experiment at CERN,” *Phys. Rev. D* **100** (2019) 035003 [[arXiv:1810.06856](#)].
- [82] L. Marsicano, *et al.*, “Dark photon production through positron annihilation in beam-dump experiments,” *Phys. Rev. D* **98** (2018) 015031 [[arXiv:1802.03794](#)].
- [83] J. D. Bjorken, *et al.*, “Search for Neutral Metastable Penetrating Particles Produced in the SLAC Beam Dump,” *Phys. Rev. D* **38** (1988) 3375.
- [84] L. Marsicano, *et al.*, “Novel Way to Search for Light Dark Matter in Lepton Beam-Dump Experiments,” *Phys. Rev. Lett.* **121** (2018) 041802 [[arXiv:1807.05884](#)].
- [85] J. D. Bjorken, R. Essig, P. Schuster, and N. Toro, “New Fixed-Target Experiments to Search for Dark Gauge Forces,” *Phys. Rev. D* **80** (2009) 075018 [[arXiv:0906.0580](#)].
- [86] S. N. Gninenko, D. V. Kirpichnikov, M. M. Kirsanov, and N. V. Krasnikov, “The exact tree-level calculation of the dark photon production in high-energy electron scattering at the CERN SPS,” *Phys. Lett. B* **782** (2018) 406–411 [[arXiv:1712.05706](#)].
- [87] Y.-S. Liu, D. McKeen, and G. A. Miller, “Validity of the Weizsäcker-Williams approximation and the analysis of beam dump experiments: Production of a new scalar boson,” *Phys. Rev. D* **95** (2017) 036010 [[arXiv:1609.06781](#)].
- [88] Y.-S. Liu and G. A. Miller, “Validity of the Weizsäcker-Williams approximation and the analysis of beam dump experiments: Production of an axion, a dark photon, or a new axial-vector boson,” *Phys. Rev. D* **96** (2017) 016004 [[arXiv:1705.01633](#)].
- [89] **Belle-II** Collaboration, “Snowmass White Paper: Belle II physics reach and plans for the next decade and beyond.” [arXiv:2207.06307](#).
- [90] **NA64** Collaboration, “Constraints on New Physics in Electron $g - 2$ from a Search for Invisible Decays of a Scalar, Pseudoscalar, Vector, and Axial Vector,” *Phys. Rev. Lett.* **126** (2021) 211802 [[arXiv:2102.01885](#)].
- [91] **Belle** Collaboration, “Precision Measurement of Charged Pion and Kaon Differential Cross

Sections in e^+e^- Annihilation at $s=10.52$ GeV,” *Phys. Rev. Lett.* **111** (2013) 062002 [[arXiv:1301.6183](#)].

- [92] C. Doglioni, *et al.*, eds., “Lepton identification in Belle II using observables from the electromagnetic calorimeter and precision trackers,” *EPJ Web Conf.* **245** (2020) 06023.
- [93] J. Alwall, *et al.*, “The automated computation of tree-level and next-to-leading order differential cross sections, and their matching to parton shower simulations,” *JHEP* **07** (2014) 079 [[arXiv:1405.0301](#)].